In-situ biosynthetic BC/zeolite hybrid hemostat for quick clot

Yang Wang
Jiangnan University
Zhuquan Li
Jiangnan University
Shiqin Liao
Jiangxi Institute of Fashion Technology
Yan Kong
Jiangnan University
Qingqing Wang
Jiangnan University
Qufu Wei (qfwei@jiangnan.edu.cn)
Jiangnan University

Research Article

Keywords: bacterial cellulose, zeolite, in-situ biosynthetic process, nanofibrous aerogels, hemostasis

Posted Date: July 19th, 2022

DOI: https://doi.org/10.21203/rs.3.rs-1841033/v1

Abstract

Zeolite-based hemostatic agents are considered as an outstanding material to achieve rapid and definitive hemostasis in pre-hospital management. However, developing a safer zeolitic hemostat that avoids the potential thrombotic risk caused by tiny zeolites residue in bleeding wounds remains a critical challenge. In this research, mesoporous zeolite particles are firmly embedded into bacterial cellulose nanofibrous aerogels (termed BC/zeolite NFAs) via an economical and eco-friendly *in-situ* biosynthetic process. After calcium ion exchange process, the BC/zeolite-Ca NFAs display efficient hemostatic properties due to their inherent high absorbency and procoagulant activity. *In vitro* hemostatic experiments indicate that the BC/zeolite-Ca NFAs can rapidly initiate and propagate the coagulation cascade to promote blood clot formation. Significantly, the blood clotting time is decreased from 7.5 ± 0.3 min to 2.2 ± 0.3 min when employing the BC/zeolite-Ca NFAs. This work demonstrates that the *in-situ* biosynthesized BC- and zeolite-based hemostats have potential applications in pre-hospital hemostasis management.

Introduction

The average blood volume of the human body (70 kg weight) is generally only 5 liters, however, it plays a crucial role in human circulatory system. For example, as a fluid connective tissue, blood is responsible for transporting gases and nutrients to tissues and organs throughout the body as well as providing immune protection and hemostatic responses as needed (Hickman, Pawlowski, Sekhon, Marks, & Gupta, 2018). Hence, blood loss can easily lead to serious consequences such as tissue morbidities and even mortalities (Blackbourne et al., 2013). However, it seems inevitable that human beings will suffer from traumatic injuries in both battlefield and civilian conditions, resulting in massive blood loss. Under such circumstances, achieving rapid and precise hemostasis in prehospital care is critical to ensuring patients survival. Fortunately, Mother Nature has provided humans with a variety of hemostatic materials that can be used to stop bleeding, such as natural polymer like cotton or chitosan and silicon-based materials like kaolin or zeolite (Bano, Arshad, Yasin, Ghauri, & Younus, 2017; Bennett & Littlejohn, 2014; Ebrahimi, Golaghaei, Mehramizi, & Morovati, 2018; Kheirabadi et al., 2010; Pourshahrestani, Zeimaran, Djordjevic, Kadri, & Towler, 2016). The various hemostatic materials have different coagulant functions due to their own active components.

In particular, zeolites have been developed for hemostatic applications due to their low cost, accessibility and non-biohazardous properties (Yu et al., 2019). Zeolites have mesoporous structures that can concentrate the blood components at the hemorrhagic site by absorbing water from the blood to facilitate clotting. Furthermore, the cage-like cavities of zeolites can accommodate positively charged Ca_2^+ ions, which further help activate the blood coagulation cascade to control bleeding (Alam et al., 2004; Shang et al., 2021). For example, granular zeolite-based hemostats were verified to be extremely effective for temporary massive bleeding control and have been commercialized, such as QuikClot (Alam et al., 2004; Kheirabadi, Scherer, Estep, Dubick, & Holcomb, 2009). Although these zeolitic hemostats seem to display tremendous potential in first aid due to their remarkable advantages, the potential risk of thermal injury

and distal thrombosis caused by such hemostats confined their application. In 2019, Jie and their group reported a tightly bonded mesoporous zeolite–cotton hybrid hemostat that not only circumvented the exothermic reaction produced by mesoporous zeolite, but also reduced the potential risk of zeolite remaining in the skin (Yu et al., 2019). However, direct contact with wound may still allow tiny mesoporous zeolites to enter blood vessels and result in thrombotic hazard. Therefore, we propose a novel structure that the mesoporous zeolites can be sandwiched and immobilized in a dense network composed of bacterial cellulose (BC) nanofibers via *in-situ* biosynthetic process.

In recent years, BC, an extracellular product biosynthesized by *Acetobacter* species, has been recognized as a desirable scaffold (Dayal & Catchmark, 2016). Actually, BC is gaining popularity in wound dressings, tissue engineering and other biomedical applications due to their high hydrophilicity, good moisture retention, excellent biocompatibility, and the simulated structure of natural extracellular matrix (Azeredo, Barud, Farinas, Vasconcellos, & Claro, 2019; Biskin et al., 2016; Portela, Leal, Almeida, & Sobral, 2019; Shen et al., 2022). The *in-situ* biosynthesis of BC is a facile, economical, and eco-friendly process which can be combined with functional additives in the culture medium to fabricate flexible nanocomposites (Sarkandi, Montazer, Harifi, & Rad, 2021; Shen et al., 2022). In particular, the natural network and porous structure formed during BC growth can provide anchoring sites and inner space for guest molecules (Almasi, Mehryar, & Ghadertaj, 2019). Furthermore, the high hydrophilicity and porous structure of BC enable fast diffusion and adsorption of water from blood to concentrate the blood components at the hemorrhagic site. In contrast to those reported zeolitic composites, the *in-situ* biosynthetic process used here not only avoids the thrombotic risk caused by zeolite leaching, but also reduces the thermal damage due to direct contact of zeolite with the skin. To our knowledge, the preparation method that immobilize mesoporous zeolite in BC networks via *in-situ* biosynthesis has yet to be reported.

Herein, we fabricated a novel zeolite- and BC-based nanofibrous aerogels for hemostatic applications through an economical and eco-friendly *in-situ* biosynthetic process. The surface morphology and section structure of the nanofibrous aerogels were observed by scanning electron microscopy (SEM), and other characterizations were analyzed by Energy-dispersive spectroscopy (EDS), Fourier transform infrared (FTIR), and X-ray diffraction (XRD), etc. The granular zeolites were tightly bonded in a dense network composed of BC nanofibers via the *in-situ* biosynthesis, which significantly improved the use safety of zeolite-based hemostatic agents. To evaluate the procoagulant activity of the biosynthesized nanofibrous aerogels, blood clotting index and hemocytes adhesion behaviors were investigated. Furthermore, the *in-vitro* blood clotting time and plasma clotting time were also measured to evaluate their hemostatic performance. Taken together, our findings demonstrate the *in-situ* biosynthesis is a promising approach to develop BC/zeolite hybrid hemostats.

Experimental

Materials

Zeolite powder (NaY, average size = 90 nm) was obtained from Nankai University Catalyst Co., Ltd (Tianjin, China). Fresh rabbit blood was obtained from Qingdao Antiserum Biotechnology Co., Ltd (Qingdao, China). The remaining chemical regents including yeast extract, peptone, mannitol, sodium hydroxide, and phosphate-buffered saline (PBS, pH = 7.4) were purchased from Sinopharm Chemical Reagent Co., Ltd (Shanghai, China). All the chemicals were used without purification.

Characterization

The morphology and structure of NaY zeolite, BC, and BC/zeolite NFAs were observed by SEM (Hitachi SU1510, Japan). The average diameters and size distributions of NaY zeolite, BC nanofibers, and pores between BC nanofibers were measured by using Nano Measurer software (Fudan University, China). XRD patterns were collected by an X-ray diffractometer (Bruker, Germany). Thermal gravimetric analysis (TGA) was characterized using a thermal analyzer at a heating rate of 20°C/min (TA Q500, Mettler Toledo, USA). Elemental mappings were recorded by using an EDAX Octane EDS-30 System (USA). The contact angle was tested by a DCAT-21 Interface Tensiometer (Dataphysics, Germany). Absorbance values in blood assay was measured by an ultraviolet spectrophotometer (UV-2600, Shimadzu Corporation, Japan).

In-situ biosynthesis of BC/zeolite NFAs

According to our previous research, *Gluconacetobacter xylinus* (ATCC 10245) was used for *in-situ* BC growth (Shen et al., 2021). Firstly, the BC medium containing 2.5% (w/v) mannitol, 0.3% (w/v) yeast extract, 0.5% (w/v) peptone, and 10 mg/mL zeolite powder was sterilized at 121℃ for 17 min, then ultrasonically dispersed for 2 h. After that, 0.9 mL of the BC medium and 0.1 mL of *G. xylinus* starter culture were mixed and incubated in a 24-well plate at 30℃. After 4 days of static incubation, the BC/zeolite nanocomposites in each well were inverted under sterile conditions and cultivated for another 4 days to further tightly fix the zeolite layer. Afterwards, the obtained BC/zeolite hydrogels were soaked in 4% sodium hydroxide solution at 80℃ for 2 h, and then washed with deionized water for 5 times. Finally, the BC/zeolite hydrogels were freeze-dried to obtain BC/zeolite NFAs, as illustrated in Fig. 1.

Calcium ion-exchange process of BC/zeolite NFAs

The BC/zeolite NFAs were immersed in 5 M $CaCl_2$ solution with slight vibration at room temperature for 12 h, and then washed in deionized water for 5 times to remove residual $CaCl_2$ solution. After that, the BC/zeolite-Ca hydrogels were freeze-dried to obtain BC/zeolite-Ca NFAs.

Blood clotting index test

The blood clotting index (BCI) was used to evaluate the hemostatic performance of samples (Wang, Ying, Zhang, Ren, & Kim, 2021). Before testing, the circular samples (Diameter = 1.5 cm) were placed in Petri dishes (Φ = 90 mm) and preheated at 37℃ for 5 min. Subsequently, 0.2 mL 0.1 mol/mL $CaCl_2$ solution was added in 1.8 mL anticoagulant whole blood with 10 s of vortex. 100 μL of the blood was immediately dripped onto each sample, and then co-incubated at 37℃ for 5 min. After that, 25 mL of

deionized water was slowly added to each Petri dish along the edge and slightly shaken at 30 rpm for 10 min. The uncoagulated red blood cells would occur hemolysis phenomenon in deionized water and appear characteristic UV-vis absorption at 540 nm. The absorbance of the sample hemoglobin solution (Abs_{sample}) and whole blood in deionized water (Abs_{blank}) were measured at 540 nm by UV-vis spectrophotometer. The BCI was calculated according to Eq. (1):

$$BCI = \frac{Abs_{sample}}{Abs_{blank}} \times 100$$

1

To further observe the micro morphology of blood clot, the tested BC/zeolite-Ca NFAs was soaked in 2.5% (w/w) glutaraldehyde/PBS solution overnight for cells fixing. Then, a series of graded alcohol solutions (50%, 60%, 70%, 80%, 90%, 95%, 100%) were used for cells dehydration. The dehydrated sample was dried at 37°C for 12 h and observed by SEM.

Red blood cells and platelets adhesion

The anticoagulant whole blood was centrifuged at 1700 rpm for 10 min, and red blood cells (RBCs) and platelet-rich plasma (PRP) were collected from red lower layer and yellowish middle layer of the centrifuged blood, respectively. 100 μL of RBCs or PRP were dropped onto samples and incubated at 37℃ for 5 min, respectively. After incubation, the samples were washed by PBS for 3 times, then soaked in 2.5% (w/w) glutaraldehyde/PBS solution overnight and gradually dehydrated by a series of graded alcohol solutions (50%, 60%, 70%, 80%, 90%, 95%, 100%). Finally, the samples were dried at 37°C overnight and observed by SEM.

Hemolysis assay

The hemolytic activities of BC, BC/zeolite, and BC/zeolite-Ca NFAs were investigated according to the reported method (Yin, Wan, Ren, & Chu, 2021). 10 mL of anticoagulant whole blood was diluted with 20 mL of PBS and centrifuged at 1500 rpm for 10 min to collect the RBCs. Then, the collected RBCs were diluted with PBS at ratio of 1:19 to prepare 5% (v/v) RBCs/PBS solution. The BC, BC/zeolite, and BC/zeolite-Ca NFAs were minced and added in PBS (10 mg/mL) solution for extraction at 37℃ for 3 h. After that, 1 mL of 5% RBCs/PBS solution was added in 2 mL of the extracted solution and co-incubated at 37℃ for another 3 h. Meanwhile, 1 mL of 5% RBCs/PBS solution was added in 2 mL of PBS solution and deionized water as negative and positive controls, respectively. Afterwards, the incubated mixtures were centrifuged at 2000 rpm for 10 min, and the absorbance of the supernatants were measured at 540 nm by a UV-vis spectrophotometer. The hemolysis (%) was calculated according to Eq. (2):

$$Hemolysis(\%) = \frac{A_{sample} - A_{negative}}{A_{positive} - A_{negative}} \times 100 \quad (2)$$

Where A_{sample}, $A_{negative}$, and $A_{positive}$ are absorbance of supernatant of the samples (BC, BC/zeolite, and BC/zeolite-Ca NFAs), PBS solution and deionized water.

In vitro whole blood clotting time and plasma clotting time assay

The circular samples (Φ = 1.5 cm) were respectively placed on the bottom of 24-well plate and preheated at 37℃ for 5 min. 0.2 mL 0.1 mol/mL $CaCl_2$ solution was added in 1.8 mL anticoagulant whole blood with 10 s of vortex, then 100 μL of the blood was dropped on each sample. Meanwhile, 100 μL of above blood added into 24-well plate without samples was used as control. Every 30 s, 2 mL of PBS solution was slowly added to each well to wash uncoagulated blood from the samples. Blood clotting time was defined as the time for a stable blood clot to form on the surface of samples. The experiment was carried out at 37℃.

In order to further evaluate the procoagulant activity, the *in vitro* plasma clotting time of the samples was tested (Yu et al., 2019). The anticoagulant whole blood was centrifuged at 1500 rpm for 10 min to collect the supernatant plasma. Then, 180 μL plasma, 20 μL $CaCl_2$, a square sample (1 × 1 cm) were sequentially added to a 1.5 mL centrifuge tube. Plasma clotting time was defined as the time for firm plasma clot which stuck to the wall of the centrifuge tube. The experiment was carried out at 37℃

Biocompatibility tests

Rat fibroblast cells (L929) were firstly resuscitated in DMEM medium containing 10% FBS and 1% penicillin-streptomycin under 5% CO_2 atmosphere at 37℃ for 12 h. Then, the resuscitated L929 cells and sterile circular sample (Φ = 1.5 cm) were seeded in two 96-well plates, respectively, and cultured for 24 h. After that, the culture medium of L929 cells was slowly sucked out and replaced with the culture medium of sample, subsequently cultured for another 24 h. The 96-well plate was measured by a Microplate reader to obtain the absorbance at 450 nm. L929 cells cultured in fresh DMEM medium served as a positive control.

Statistical analysis

The ANOVA and Student's t-test were used for statistical analysis. All the experimental data were expressed as mean ± standard deviation. The differences were considered statistically significant when $P < 0.05$.

Results And Discussion

Morphological observations

In this research, commercial NaY zeolites were selected as the hemostatic components for the *in-situ* biosynthesis process. As shown in Fig. 2a, the SEM image of NaY zeolites showed micro-nano size with an average diameter of 784.6 ± 137.8 nm and the right histogram displayed the diameter distribution of

NaY zeolites (520–1300 nm). The SEM image in Fig. 2b showed the typical 3D nanoscale network structure of freeze-dried BC/zeolite NFAs, consisting of BC nanofibers with an average diameter of 75.2 ± 20.5 nm. Besides, the irregular pores were observed in Fig. 2b, which were formed during freeze-drying process due to the sublimation of ice encapsulated in the BC nanofibrous network (Wu & Meredith, 2014). These pores with an average dimeter of 230.9 ± 77.5 nm and a distribution ranging from 90 to 430 nm, were smaller than the size of NaY zeolites. In Fig. 2c (left), the cross-section of BC/zeolite NFAs exhibited a sandwich-like structure, in which the zeolite particles were tightly encapsulated in interlayer by BC nanofiber layers on both sides. By using a higher magnification (Fig. 2c right), the structure of zeolite particles entangled with BC nanofibers was observed, which might further enhance the binding force between zeolites and BC nanofibers. These results demonstrated a sandwich-like structure that NaY zeolite particles were firmly embedded into BC nanofibrous networks via *in-situ* biosynthetic process.

In order to further confirm the inherent sandwich-like structure, EDS analysis was performed on the cross-section of the BC/zeolite-Ca NFAs. As shown in Fig. 3, the SEM image was consistent with Fig. 2c, confirming the good stability of the sandwich-like structure. On the other hand, the spot signals in C element mapping formed two well-defined outer-layers, corresponding to the BC layers in the SEM image. Meanwhile, the spot signals distribution in O element mapping indicated that the O was presented in whole BC/zeolite-Ca NFAs. However, the spot signals of Al, Si, and Ca formed a clearly defined meddle-layer in their element mappings, respectively, corresponding to the zeolite-Ca layer in the SEM image.

Characterization of BC/zeolite NFAs

As seen in Fig. 4a, the FTIR spectrum was used to characterize the functional groups of zeolite, BC, and BC/zeolite composites. The characteristic peaks of BC around 3343 cm^{-1}, 2895 cm^{-1}, and 1055 cm^{-1} were ascribed to -OH, -CH_2, and C-O-C stretching vibrations (Li et al., 2017). Compared with BC spectrum, the characteristic peak at 790 cm^{-1} was only found in zeolite and BC/zeolite composites spectra, which was associated with Si-O-Al groups in zeolite particles (Salim & Malek, 2016). The crystallinity of the purchased and biosynthesized materials was investigated by XRD (Fig. 4b). The purchased zeolite particles showed intense peaks at 2θ = 6.25°, 15.75°, 23.75°, 27.15°, and 31.50°, which confirmed the typical faujasite (IZA) structure of NaY zeolite phase (Salim & Malek, 2016). Meanwhile, these characteristic diffraction peaks were found in BC/zeolite and BC/zeolite-Ca spectra, and showed no significant changes, indicating that the *in-situ* biosynthetic process and calcium ion-exchanged process did not affect the crystallinity of NaY zeolite. The biosynthesized BC showed three characteristic diffraction peaks at 2θ = 14.9°, 17.2°, and 23.1°, whereas these peaks were not found in BC/zeolite and BC/zeolite-Ca spectra, which might be attributed to the weaker intensity of BC characteristic peaks and the less content in BC/zeolite composites (Li et al., 2017). Thus, TGA was performed to investigate the respective proportions of BC and zeolite in the BC/zeolite composite (Fig. 4c). As seen in TGA and DTG curves, the weight loss from 30℃ to 200℃ was mainly caused by water evaporation. The decomposition of BC started at around 295℃ and ended at around 400℃, and the weight loss was about 14.2%. In addition, the TGA curves exhibited a minor weight loss from 400℃ to 800℃, which might be due to the presence of -OH groups on the zeolite (Chaibi, Boucheffa, & Bendjaballah-Lalaoui, 2021). According to the

TGA, the zeolite loading in biosynthesized BC/zeolite NFAs was 82.6 ± 5.7wt% (measured from five TGA data), indicating the high loading ability via *in-situ* biosynthesis.

To investigate the stability of the BC/zeolite NFAs, we tested the residual weight of zeolite after three different treatments, including sonication for 10 min, soaking for 24 h, and stirring for 24 h. As shown in Fig. 4d, after processing in the three ways, the residual weights of zeolite were 95.4 ± 2.7%, 99.9 ± 0.1%, and 98.6 ± 1.2%, respectively, manifesting that the zeolite particles were firmly anchored into the BC nanofibers. The swelling ratios of BC, BC/zeolite, and BC/zeolite-Ca NFAs were measured and exhibited in Fig. 4e. BC NFAs displayed rapid water absorption from 0 to 10 min, and sustained absorption to a maximum value (3152 ± 111%) within two hours. For BC/zeolite and BC/zeolite-Ca NFAs, the swelling ratios exhibited similar curves to that of BC NFAs but showed lower values at the same testing moments. Not surprisingly, the embedded zeolite particles with lower absorption than BC significantly increased the weight of BC/zeolite and BC/zeolite-Ca NFAs. In addition, the swelling ratios of BC/zeolite-Ca were slightly lower than BC/zeolite, which may be ascribed to the porosity reduction of BC NFAs during continuous freeze-drying process. As shown in Fig. 4f, we recorded the images of fresh blood dropping onto BC/zeolite-Ca NFAs within 30 s, to further observe the blood absorption behavior of the aerogel. Upon contact, the blood droplet immediately spread onto the BC/zeolite-Ca NFAs and was rapidly and completely absorbed. Remarkably, the average pores size of BC layer (230.9 ± 77.5 nm) was far smaller than hemocytes including RBCs and platelets (Guo, Dong, Bang, & Li, 2021). Therefore, we speculate that the water in the blood is absorbed, but most of the blood components are concentrated and assembly onto the BC/zeolite-Ca NFAs.

BCI and hemolysis assay, and hemocytes adhesion

The BCI assay was used to assess the procoagulant activity of the hemostats, with lower BCI values generally indicating better procoagulant performances (Yin et al., 2020). The BCI values were measured when the whole blood contacted with hemostats for 5 min, and the results were shown in Fig. 5a. In comparison with the blank control (BCI = 100 ± 1.0), the BCI value of BC NFAs decreased to 82.0 ± 1.8. It demonstrated that BC NFAs could absorb the water from blood and concentrate the blood components to promote blood clotting (Edwards & Prevost, 2011). BC/zeolite NFAs displayed a lower BCI value (73.6 ± 1.2) than BC NFAs, which probably caused by the release of Na^+ from NaY zeolites (Yu et al., 2021). After calcium ion-exchange process, the BCI value of BC/zeolite-Ca NFAs dropped significantly to 27.3 ± 1.5, displaying the best procoagulant performance in the assay. As we know, zeolite is a kind of microporous aluminosilicate that can accommodate Ca^{2+} during calcium ion-exchange process, which play a significant role in blood coagulation cascade (Shang et al., 2021). Based on this, we believe that the strong water absorption and Ca^{2+} release of BC/zeolite-Ca NFAs are two crucial factors in prompting the procoagulant performance. In addition, the BC NFAs were treated via calcium ion-exchange process, labeled as BC-Ca. The BC-Ca exhibited a similar BCI value to BC, manifesting that BC has no capacity for Ca^{2+} exchange. Thus, the BC-Ca NFAs will not be further evaluated and discussed later.

The hemolysis activity assay was used to evaluate the hemocompatibility of hemostats. In general, an ideal and safe hemostat should induce less than 5% hemolysis after contact with blood cells (Peng et al., 2021). As shown in the inset in Fig. 5b, all the NFAs displayed transparent supernatants similar to PBS (negative control), while the DI water (positive control) displayed a red supernatant. It demonstrated that the RBCs were ruptured in DI water, whereas the RBCs remained intact after contacted with these NFAs or in PBS. Furthermore, the hemolysis ratios of BC, BC/zeolite, and BC/zeolite-Ca NFAs were all less than 5%, manifesting that these NFAs possessed good hemocompatibility.

To further reveal the hemostatic mechanism, the micro morphology of whole blood clot (Fig. 5c), RBCs adhesion (Fig. 6a), and platelets adhesion (Fig. 6b) were observed by SEM. As shown in Fig. 5c, a large number of hemocytes and plasma components aggregated on the surface of BC/zeolite-Ca NFAs, forming a stable blood clot. Besides, massive RBCs (red arrows) and multi-tentacled platelets (blue arrows) were observed in this magnified SEM image. The SEM images in Fig. 6a showed the adhesion of RBCs to BC NFAs and BC/zeolite-Ca NFAs, and more RBCs were observed on BC/zeolite-Ca NFAs than on BC NFAs. We presume that the positively charged Ca^{2+} released from BC/zeolite-Ca NFAs could significantly enhance the hemagglutination reaction. Furthermore, comparing the morphologies of platelets on BC NFAs and BC/zeolite-Ca NFAs in Fig. 6b, it was obvious that the platelets on BC/zeolite-Ca NFAs deformed and stretched out a lot of spiny pseudopodia. This phenomenon indicated that the platelets could be activated on BC/zeolite-Ca NFAs but not on BC NFAs. In the platelet adhesion test, PRP was obtained from anticoagulant blood, thus Ca^{2+} released from BC/zeolite-Ca NFAs could neutralize the anticoagulants in PRP and further participate in the activation process of platelets (Yeung, Yamashita, & Prakriya, 2017).

In vitro clotting time assay

In vitro blood clotting performances of BC, BC/zeolite, and BC/zeolite-Ca NFAs were evaluated by monitoring the clotting time of whole blood and plasma (Fig. 7). As seen in Fig. 7a, the clotting time of whole blood was 7.5 ± 0.3 min in the absence of any hemostatic material. After contact with BC and BC/zeolite NFAs, the clotting time decreased to 6.5 ± 0.3 min and 6.4 ± 0.4 min, respectively, which could be ascribed to the strong absorbability of the BC or BC/zeolite NFAs. After contact with BC/zeolite-Ca NFAs, the clotting time dramatically decreased to 2.2 ± 0.3 min, due to BC/zeolite-Ca NFAs could rapidly absorb the water form blood to concentrate the blood components and release Ca^{2+} to further accelerate the coagulation cascade. The results of plasma clotting time displayed a similar regularity to that of whole blood. As seen in Fig. 7b, the clotting time of plasma was 10.7 ± 0.2 min in the absence of any hemostatic material, which was longer than that of whole blood. This phenomenon could be attributed to the lack of platelets in plasma to participate in the coagulation cascade (Yu et al., 2021). It was worth noting that the plasma clotting time decreased to 7.2 ± 0.4 min and 7.1 ± 0.4 min after adding BC NFAs and BC/zeolite NFAs into the centrifuge tubes, respectively. After adding BC/zeolite-Ca NFAs into the centrifuge tubes, the plasma clotting time decreased more significantly to 2.4 ± 0.2 min. In addition, as seen in Fig. 7b, the optical images displayed the whole blood clot and plasma clots at the test time of 2.5 min. Due to the rapid hemostatic effect of BC/zeolite-Ca NFAs, the stable whole blood and plasma clot

were formed and firmly stuck to the surface of the aerogel and the wall of the centrifuge tube, respectively. These results demonstrated that the BC/zeolite-Ca NFAs possessed excellent hemostatic properties to reduce blood loss in emergency situations.

Biocompatibility evaluation

Rat fibroblast cells (L929) were utilized to evaluate the biocompatibility of these NFAs. As seen in Fig. 8a, the cell viability of BC NFAs, BC/zeolite NFAs, and BC/zeolite-Ca NFAs were 94.9 ± 3.3%, 94.4 ± 1.6%, and 94.7 ± 6.9%, respectively. The results indicated that the extracts of the three kinds of NFAs were not cytotoxic. In addition, the morphologies of L929 cells after co-cultured with the extracts of BC/zeolite-Ca NFAs were observed by fluorescence staining. As shown in Fig. 8b, the live cells were stained green and exhibited oval or spindle like morphologies in the two groups (control and BC/zeolite-Ca). The BC/zeolite-Ca group showed a similar live situation of L929 cells to the control group, manifesting that BC/zeolite-Ca NFAs possessed good cytocompatibility. In conclusion, the results of cell viability and fluorescence staining assay prove that the *in-situ* biosynthetic and Ca^{2+} exchanged BC/zeolite-Ca NFAs were biocompatible and can be used as hemostats.

Hemostatic mechanisms of BC/zeolite-Ca NFAs

The hemostatic mechanisms involving concentration of blood components and activation of coagulation cascade on the surface of BC/zeolite-Ca hemostat is presented in Fig. 9. Owing to the high absorbability of BC/zeolite-Ca NFAs, the water in blood can be rapidly absorbed and result in the concentration of blood components when blood contacts with the NFAs. Notably, the blood components, such as platelets and prothrombin can easily contact or close proximity to interlayered zeolite-Ca hemostatic agents due to the 3D porous structure of outer BC nanofibers. The granular zeolite-Ca can effectively initiate and propagate the coagulation cascade via the intrinsic coagulation pathway, leading to the formation of fibrin clot (Shang et al., 2021). In addition, calcium ions released from zeolite-Ca can accelerate platelets activation, and the activated platelets rapidly adhere and aggregate blood cells and other blood components to form a firm thrombus. The thrombus that quickly forms at a bleeding wound can arrest flow of blood components to achieve hemostasis.

Conclusion

In summary, we prepared zeolite-embedded bacterial cellulose (BC/zeolite) NFAs by economical and environment-friendly *in-situ* biosynthesis. After calcium ion-exchange process, the BC/zeolite-Ca NFAs exhibited outstanding hemostatic performance due to the highly absorbent porous BC and embedded procoagulant zeolite-Ca. Upon covering the bleeding wound, the BC/zeolite-Ca NFAs can rapidly absorb the water from blood to concentrate the coagulating components and effectively initiate and propagate the coagulation cascade to accelerate thrombosis. Typically, the blood clotting time significantly decreased from 7.5 ± 0.3 min to 2.2 ± 0.3 min after employing the BC/zeolite-Ca hemostats. In addition, the sandwich-like structure of BC/zeolite-Ca NFAs, with granular zeolites were tightly embedded into BC

nanofibers, can significantly reduce the distal thrombosis risks caused by zeolite leakage. The hemolysis and cytotoxicity assessments also demonstrate the good biocompatibility of the BC/zeolite-Ca NFAs. Owing to rapid and effective hemostatic performance, safety, low cost, and environment-friendly, we believe that the *in-situ* biosynthesized BC/zeolite-Ca NFAs have great potential for bleeding control in wound dressings.

Declarations

Ethics approval and consent to participate

The experimental operations were carried out in accordance with the "*Administrative Regulations on Laboratory Animals*" of the *Ministry of Science and Technology* of the People's Republic of China.

Consent for publication

All authors agree to publication.

Availability of data and materials

All the data and materials in this manuscript are available.

Competing interests

There are no conflicts to declare.

Funding

This work was financially supported by Postgraduate Research & Practice Innovation Program of Jiangsu Province (KYCX22_2340).

Authors' contributions –

Yang Wang, Qufu Wei, and Qingqing Wang wrote the main manuscript text. Zhuquan Li prepared BC/zeolite NFAs and Yan Kong did biocompatibility tests. Shiqin Liao provided part of lab supplies. All authors reviewed the manuscript.

Acknowledgments

This work was financially supported by the National Natural Science Foundation of China (No. 51603090), supported by Postgraduate Research & Practice Innovation Program of Jiangsu Province (KYCX22_2340), Jiangxi Provincial Natural Science Foundation (No. 20212BAB214016), China Postdoctoral Science Foundation (No. 2018), International Science and Technology Center (No. BZ2018032).

References

1. Alam HB, Chen Z, Jaskille A, Querol RI, Koustova E, Inocencio R, Conran R, Seufert A, Ariaban N, Toruno K, Rhee P (2004) Application of a zeolite hemostatic agent achieves 100% survival in a lethal model of complex groin injury in Swine. J Trauma 56(5):974–983. https://doi.org/10.1097/01.ta.0000127763.90890.31
2. Almasi H, Mehryar L, Ghadertaj A (2019) Characterization of CuO-bacterial cellulose nanohybrids fabricated by in-situ and ex-situ impregnation methods. Carbohydr Polym 222. https://doi.org/10.1016/j.carbpol.2019.114995
3. Azeredo HMC, Barud H, Farinas CS, Vasconcellos VM, Claro AM (2019). Bacterial Cellulose as a Raw Material for Food and Food Packaging Applications. Front Sustain Food S 3. https://doi.org/10.3389/fsufs.2019.00007
4. Bano I, Arshad M, Yasin T, Ghauri MA, Younus M (2017) Chitosan: A potential biopolymer for wound management. Int J Biol Macromol 102:380–383. https://doi.org/10.1016/j.ijbiomac.2017.04.047
5. Bennett BL, Littlejohn L (2014) Review of New Topical Hemostatic Dressings for Combat Casualty Care. Mil Med 179(5):497–514. https://doi.org/10.7205/Milmed-D-13-00199
6. Biskin S, Damar M, Oktem SN, Sakalli E, Erdem D, Pakir O (2016) A new graft material for myringoplasty: bacterial cellulose. Eur Arch Oto-Rhino-L 273(11):3561–3565. https://doi.org/10.1007/s00405-016-3959-8
7. Blackbourne LH, Baer DG, Eastridge BJ, Kheirabadi B, Kragh JF, Cap AP et al (2013). Military medical revolution: Prehospital combat casualty care. J Trauma Acute Care Surg 74(2):705–705. https://doi.org/10.1097/TA.0b013e31828174f3
8. Chaibi A, Boucheffa Y, Bendjaballah-Lalaoui N (2021) TGA investigation of water and ethanol adsorption over LTA zeolites. Micropor Mesopor Mat 324. https://doi.org/10.1016/j.micromeso.2021.111285
9. Dayal MS, Catchmark JM (2016) Mechanical and structural property analysis of bacterial cellulose composites. Carbohydr Polym 144:447–453. https://doi.org/10.1016/j.carbpol.2016.02.055
10. Ebrahimi M, Golaghaei A, Mehramizi A, Morovati A (2018) Design and Formulation of Inorganic Dispersed Organogel for Hemostasis. J Res Med Dent Sci 6(2):18–23. https://doi.org/10.5455/jrmds.2018624
11. Edwards JV, Prevost N (2011) Thrombin production and human neutrophil elastase sequestration by modified cellulosic dressings and their electrokinetic analysis. J Funct Biomater 2(4):391–413. https://doi.org/10.3390/jfb2040391
12. Guo BL, Dong RN, Bang YP, Li M (2021) Haemostatic materials for wound healing applications. Nat Rev Chem 5(11):773–791. https://doi.org/10.1038/s41570-021-00323-z
13. Hickman DA, Pawlowski CL, Sekhon UDS, Marks J, Gupta A (2018) Biomaterials and Advanced Technologies for Hemostatic Management of Bleeding. Adv Mater 30(36). https://doi.org/10.1002/adma.201804635

14. Kheirabadi BS, Mace JE, Terrazas IB, Fedyk CG, Estep JS, Dubick MA, Blackbourne LH (2010) Safety Evaluation of New Hemostatic Agents, Smectite Granules, and Kaolin-Coated Gauze in a Vascular Injury Wound Model in Swine. J Trauma 68(5):1263–1263. https://doi.org/10.1097/TA.0b013e3181dc9734
15. Kheirabadi BS, Scherer MR, Estep JS, Dubick MA, Holcomb JB (2009) Determination of Efficacy of New Hemostatic Dressings in a Model of Extremity Arterial Hemorrhage in Swine. J Trauma 67(3):450–460. https://doi.org/10.1097/TA.0b013e3181ac0c99
16. Li GH, Nandgaonkar AG, Habibi Y, Krause WE, Wei QF, Lucia LA (2017) An environmentally benign approach to achieving vectorial alignment and high microporosity in bacterial cellulose/chitosan scaffolds. Rsc Adv 7(27):16737–16737. https://doi.org/10.1039/c7ra90040f
17. Peng X, Xia X, Xu X, Yang X, Yang B, Zhao P et al (2021) Ultrafast self-gelling powder mediates robust wet adhesion to promote healing of gastrointestinal perforations. Sci Adv, 7(23). https://doi.org/10.1126/sciadv.abe8739
18. Portela R, Leal CR, Almeida PL, Sobral RG (2019) Bacterial cellulose: a versatile biopolymer for wound dressing applications. Microb Biotechnol 12(4):586–610. https://doi.org/10.1111/1751-7915.13392.
19. Pourshahrestani S, Zeimaran E, Djordjevic I, Kadri NA, Towler MR (2016) Inorganic hemostats: The state-of-the-art and recent advances. Mat Sci Eng C-Mater 58:1255–1268. https://doi.org/10.1016/j.msec.2015.09.008
20. Salim MM, Malek NANN (2016) Characterization and antibacterial activity of silver exchanged regenerated NaY zeolite from surfactant-modified NaY zeolite. Mat Sci Eng C-Mater 59:70–77. https://doi.org/10.1016/j.msec.2015.09.099
21. Sarkandi AF, Montazer M, Harifi T, Rad MM (2021) Innovative preparation of bacterial cellulose/silver nanocomposite hydrogels: In situ green synthesis, characterization, and antibacterial properties. J Appl Polym Sci 138(6). https://doi.org/10.1002/app.49824
22. Shang XQ, Chen H, Castagnola V, Liu K, Boselli L, Petseva V et al (2021) Unusual zymogen activation patterns in the protein corona of Ca-zeolites. Nat Catal 4(7):607–614. https://doi.org/10.1038/s41929-021-00654-6
23. Shen HY, Jiang CY, Li W, Wei QF, Ghiladi RA, Wang QQ (2021) Synergistic Photodynamic and Photothermal Antibacterial Activity of In Situ Grown Bacterial Cellulose/MoS_2-Chitosan Nanocomposite Materials with Visible Light Illumination. Acs Appl Mater Inter 13(26):31193–31205. https://doi.org/10.1021/acsami.1c08178
24. Shen HY, Liao SQ, Jiang CY, Zhang JW, Wei QF, Ghiladi RA, Wang QQ (2022) In situ grown bacterial cellulose/MoS_2 composites for multi-contaminant wastewater treatment and bacteria inactivation. Carbohydr Polym 277. https://doi.org/10.1016/j.carbpol.2021.118853
25. Wang Y, Ying ML, Zhang M, Ren XH, Kim IS (2021) Development of Antibacterial and Hemostatic PCL/Zein/ZnO-Quaternary Ammonium Salts NPs Composite Mats as Wound Dressings. Macromol Mater Eng 306(12). https://doi.org/10.1002/mame.202100587

26. Wu J, Meredith JC (2014) Assembly of Chitin Nanofibers into Porous Biomimetic Structures via Freeze Drying. Acs Macro Lett 3(2):185–190. https://doi.org/10.1021/mz400543f
27. Yeung PSW, Yamashita M, Prakriya M (2017) Pore opening mechanism of CRAC channels. Cell Calcium 63:14–19. https://doi.org/10.1016/j.ceca.2016.12.006
28. Yin ML, Wan SS, Ren XH, Chu CC (2021) Development of Inherently Antibacterial, Biodegradable, and Biologically Active Chitosan/Pseudo-Protein Hybrid Hydrogels as Biofunctional Wound Dressings. Acs Appl Mater Inter 13(12):14701–14712. https://doi.org/10.1021/acsami.0c21680
29. Yin ML, Wang YF, Zhang Y, Ren XH, Qiu YY, Huang TS (2020) Novel quaternarized N-halamine chitosan and polyvinyl alcohol nanofibrous membranes as hemostatic materials with excellent antibacterial properties. Carbohydr Polym 232. https://doi.org/10.1016/j.carbpol.2019.115823
30. Yu LS, Shang XQ, Chen H, Xiao LP, Zhu YH, Fan J (2019) A tightly-bonded and flexible mesoporous zeolite-cotton hybrid hemostat. Nat Commun 10. https://doi.org/10.1038/s41467-019-09849-9
31. Yu LS, Yu B, Chen H, Shang XQ, He M, Lin MC et al (2021) Highly efficient artificial blood coagulation shortcut confined on Ca-zeolite surface. Nano Res 14(9):3309–3318. https://doi.org/10.1007/s12274-021-3394-z

Figures

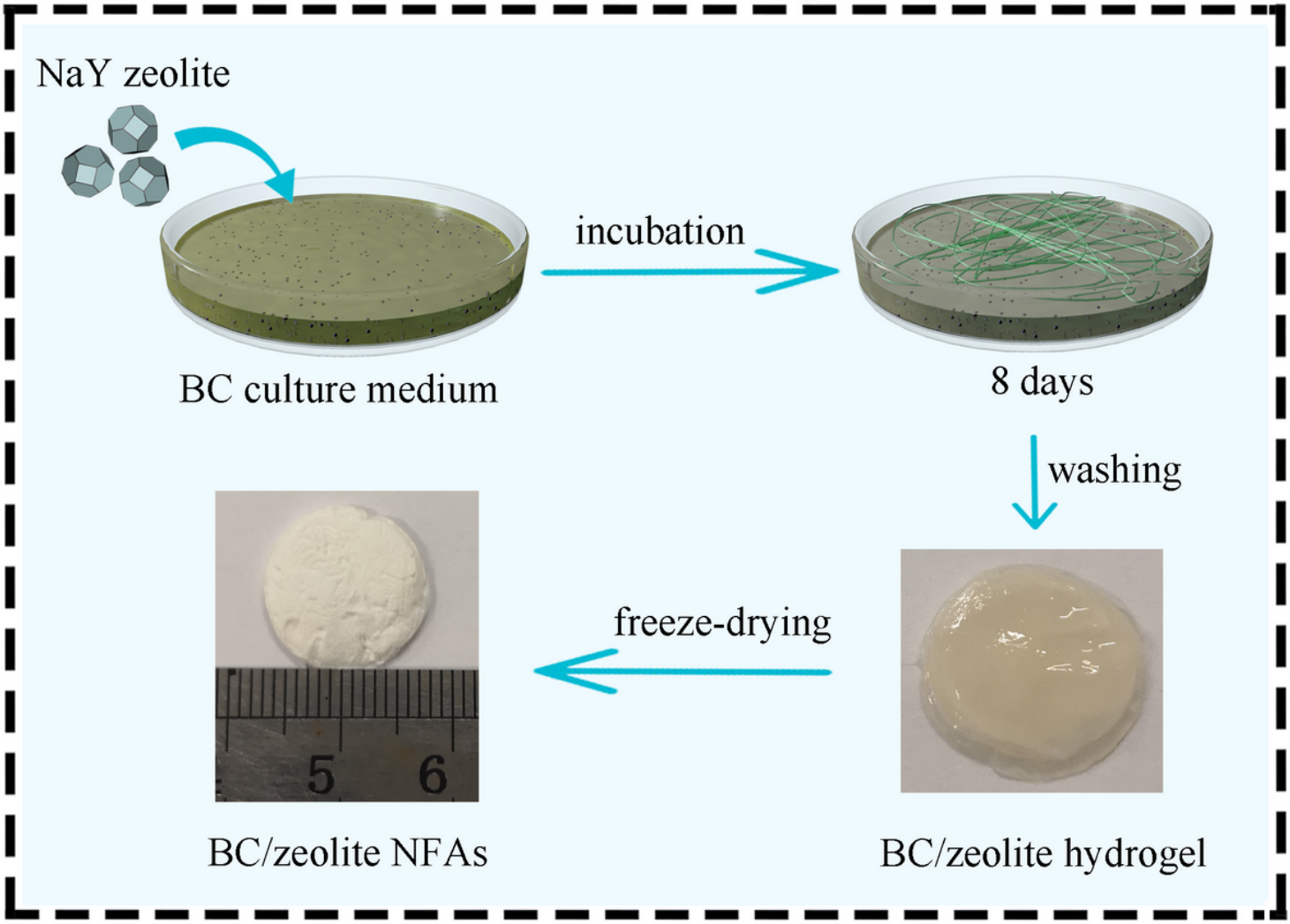

Figure 1

Schematic illustration of the *in-situ* biosynthesis of BC/zeolite NFAs.

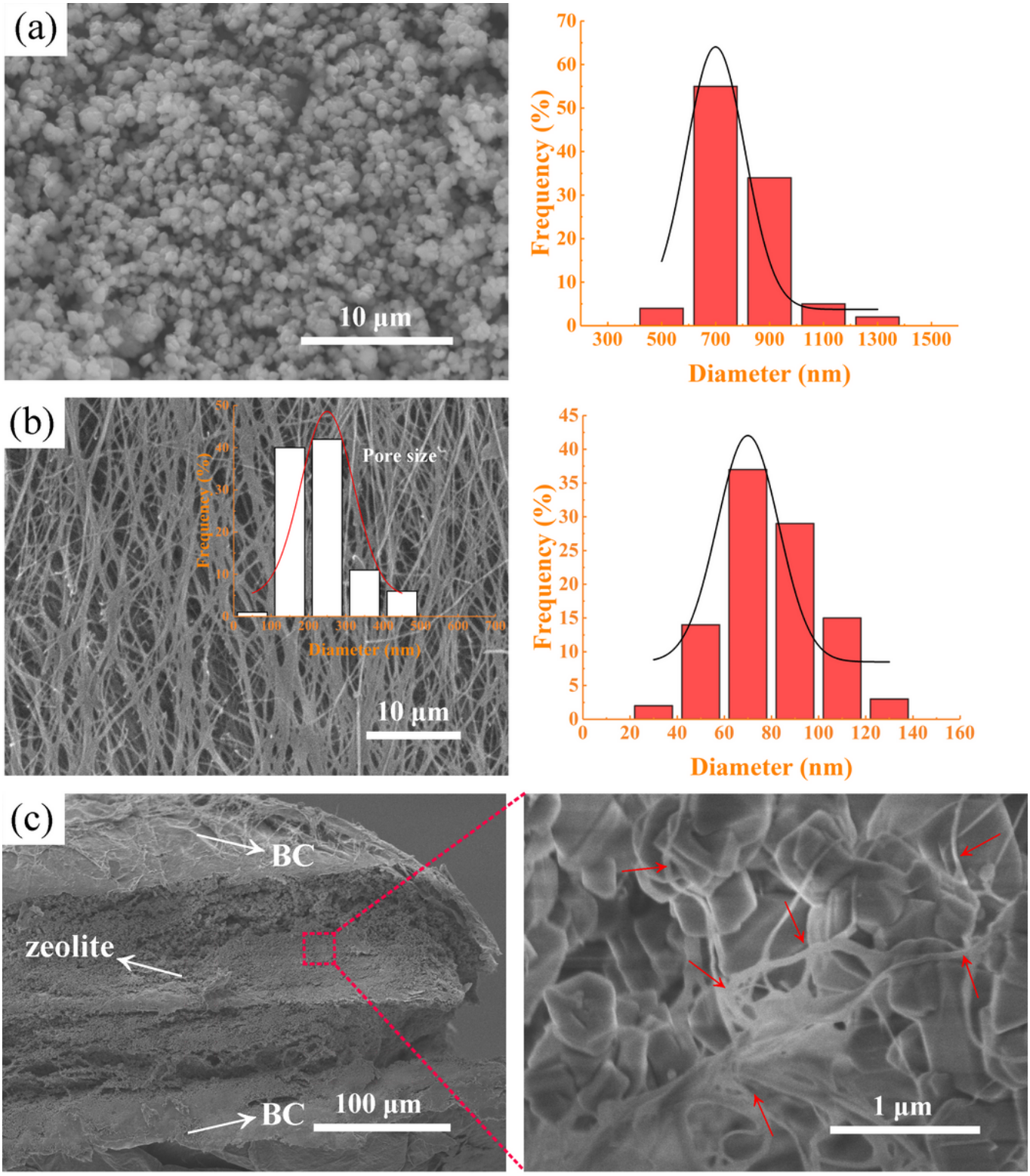

Figure 2

(a) SEM image of NaY zeolites and diameter distribution. (b) SEM image of BC/zeolite NFAs surface and diameter distribution. (c) Cross-sectional SEM image of BC/zeolite NFAs (left) and interlayer (right), with red arrows depicting the BC nanofibers.

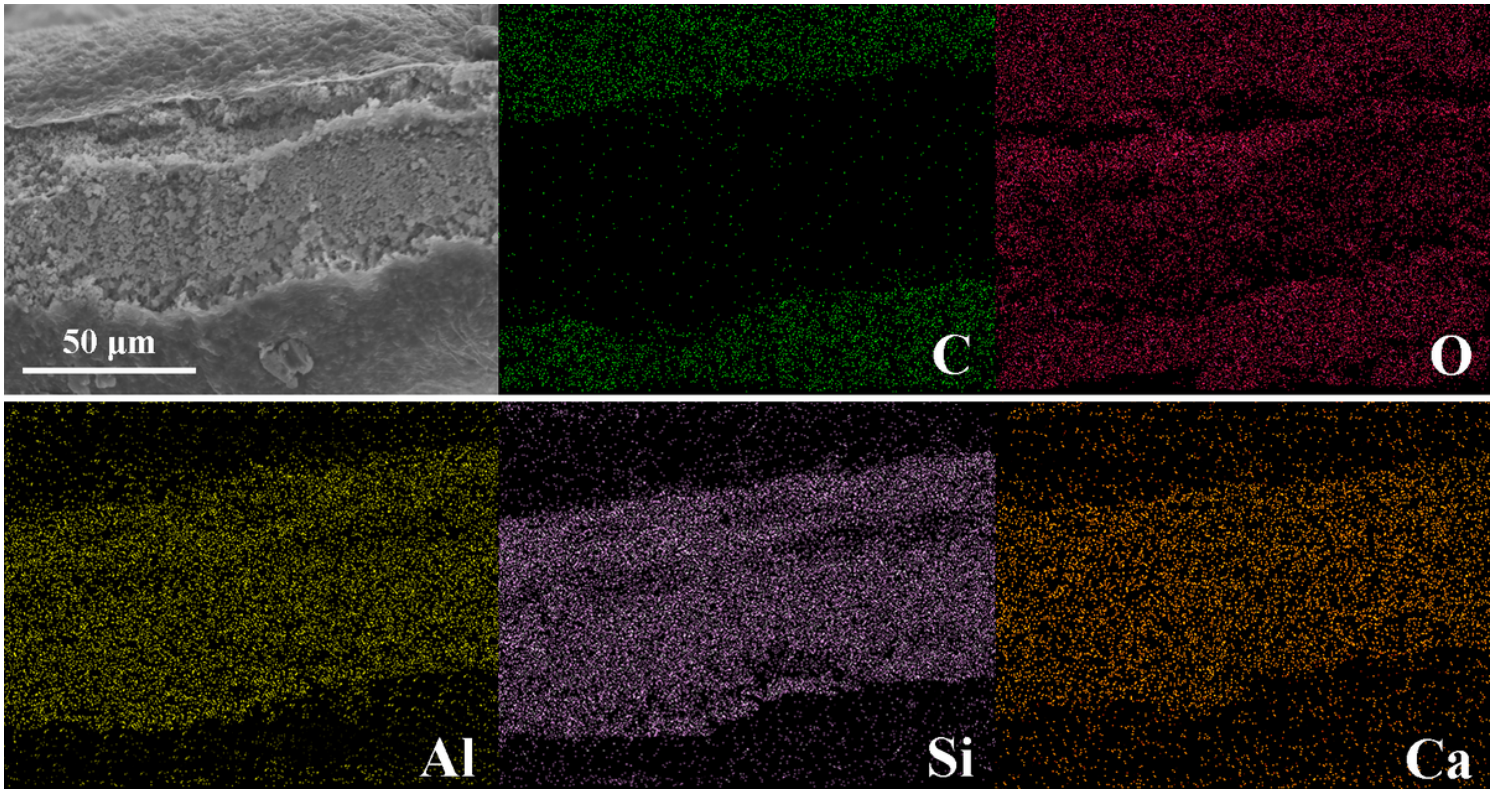

Figure 3

Cross-sectional SEM image of BC/zeolite-Ca NFAs and elemental mappings of C, O, Al, Si, and Ca.

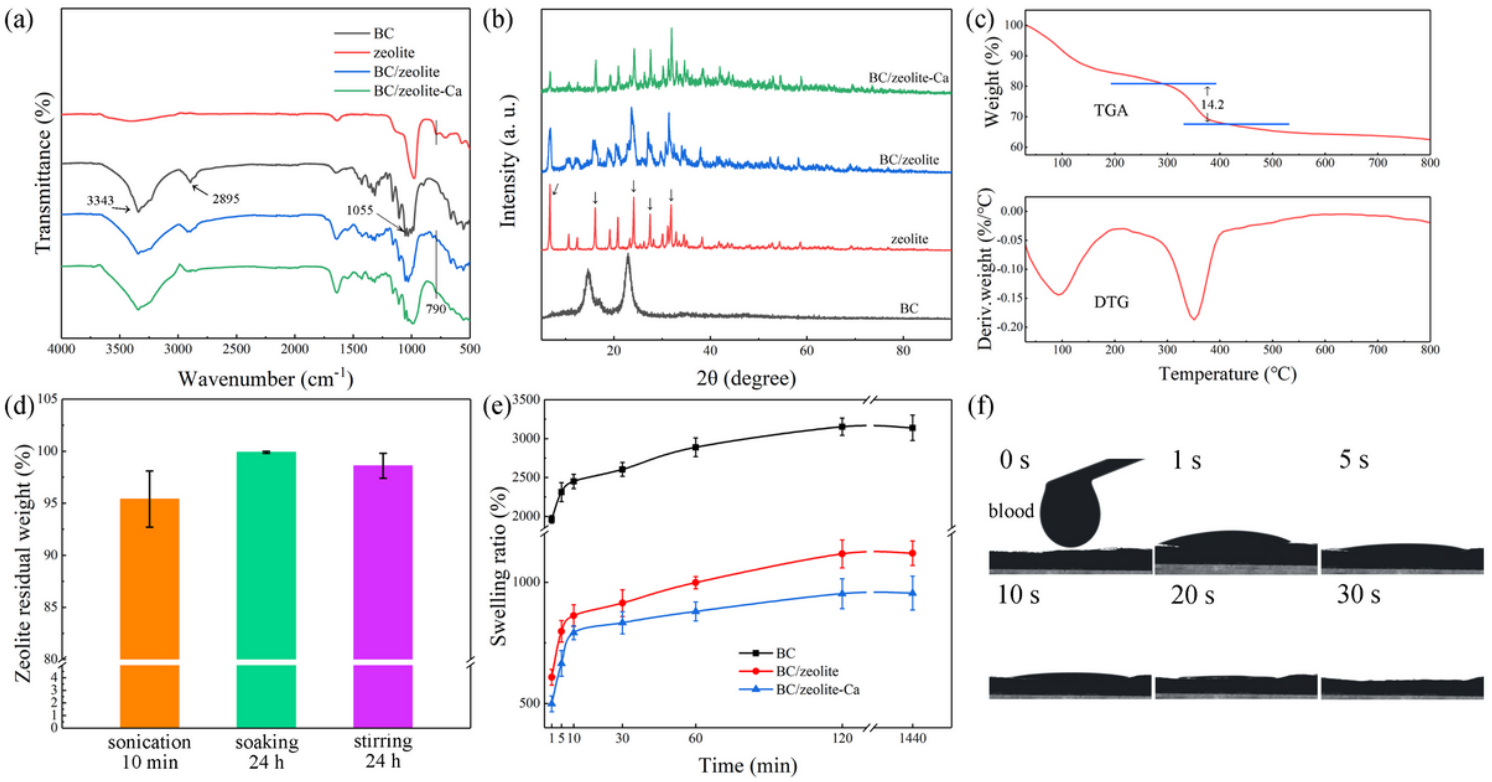

Figure 4

(a) FTIR spectra. (b) XRD analysis. (c) TGA curve and DTG of BC/zeolite. (d) Zeolite residual weight of BC/zeolite after three different treatments. (e) Swelling ratio of BC, BC/zeolite, and BC/zeolite-Ca. (d) Blood absorption behavior within 30 s.

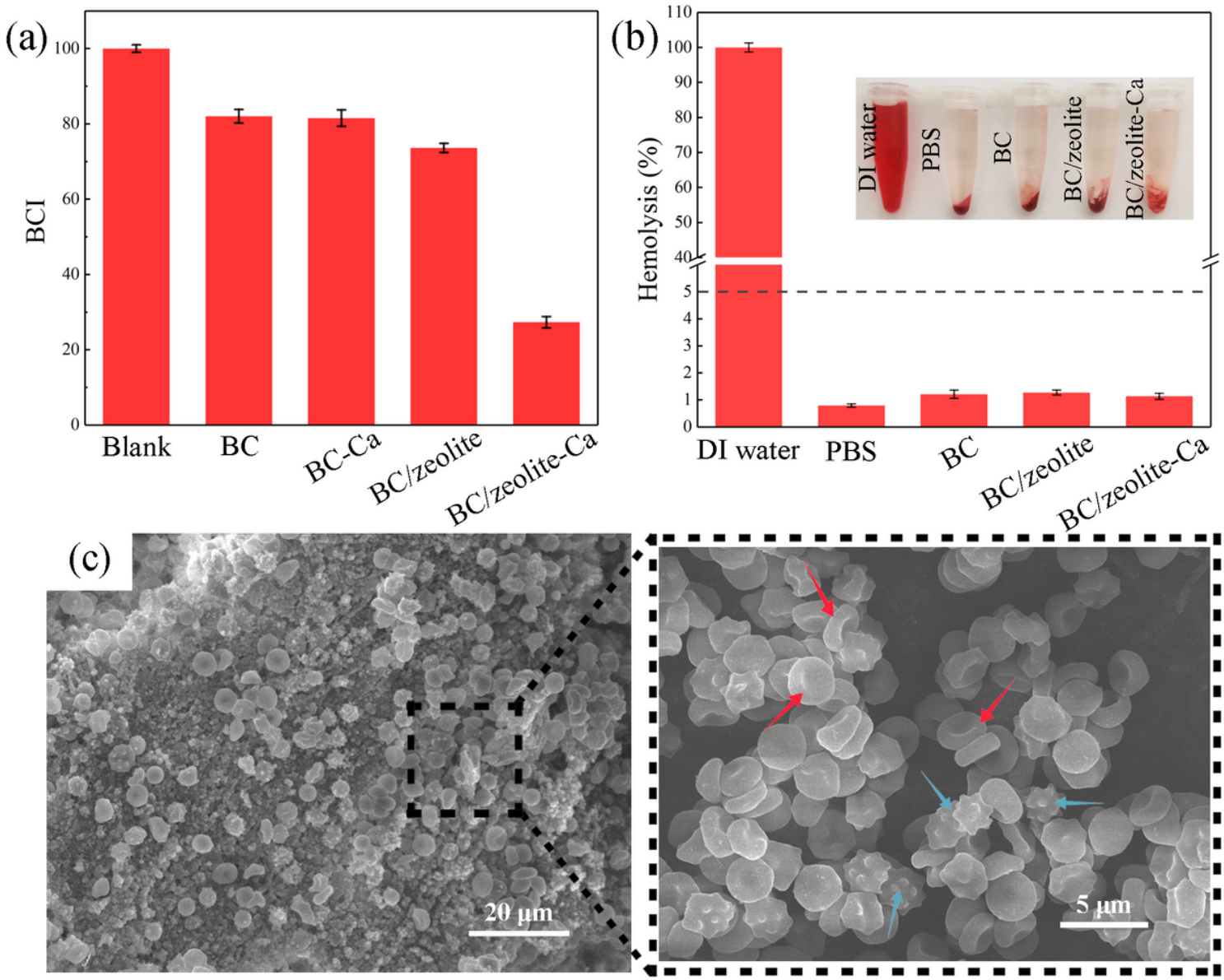

Figure 5

(a) BCI value of blank control, BC, BC-Ca, BC/zeolite, and BC/zeolite-Ca NFAs. (b) Hemolysis ratio of positive control (DI water), negative control (PBS), BC, BC/zeolite, and BC/zeolite-Ca NFAs. (c) SEM image of whole blood clot on BC/zeolite-Ca NFAs, with the red arrows representing RBCs and the blue arrows representing platelets.

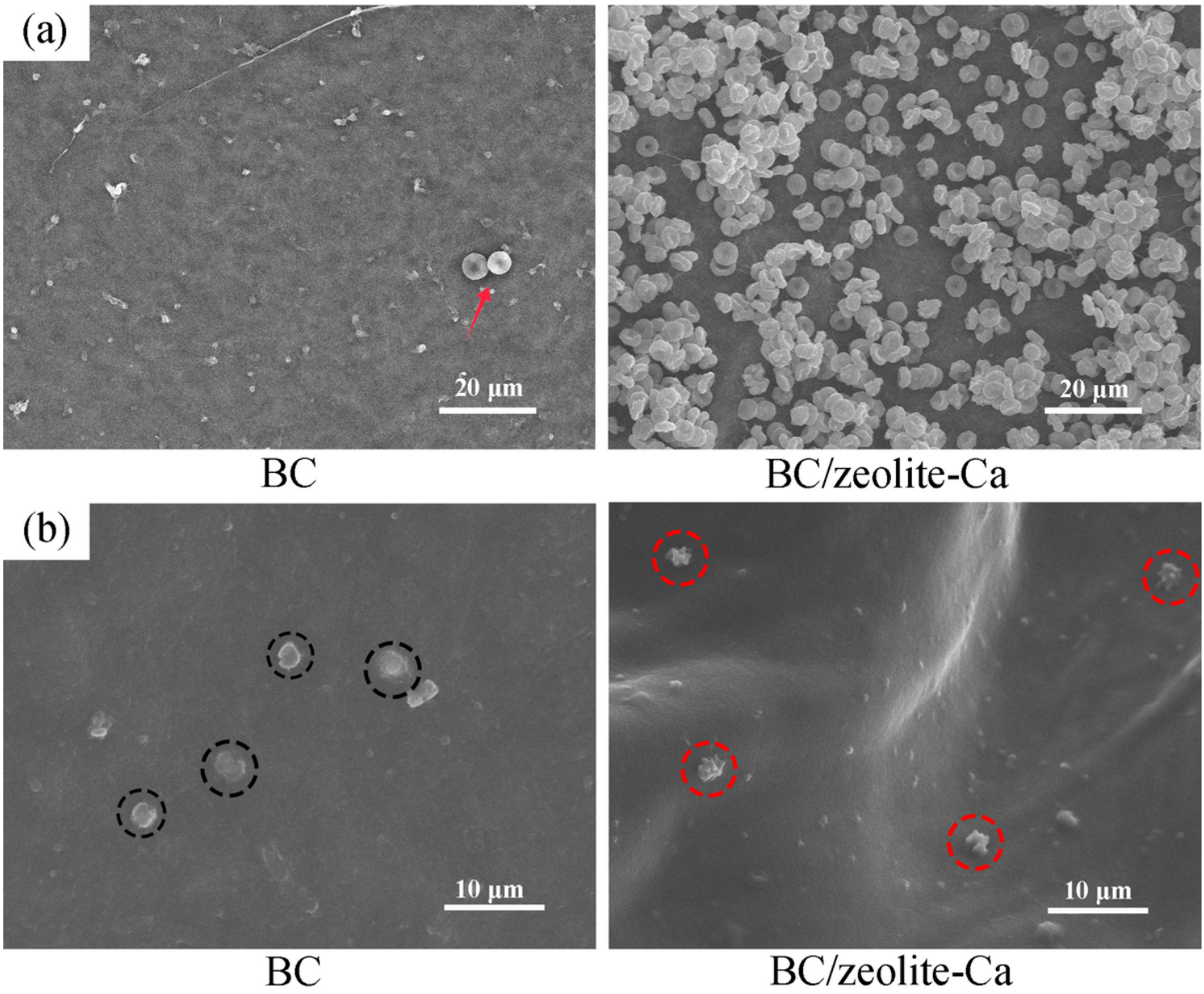

Figure 6

(a) SEM images of RBCs and platelets adhering to BC NFAs and BC/zeolite-Ca NFAs.

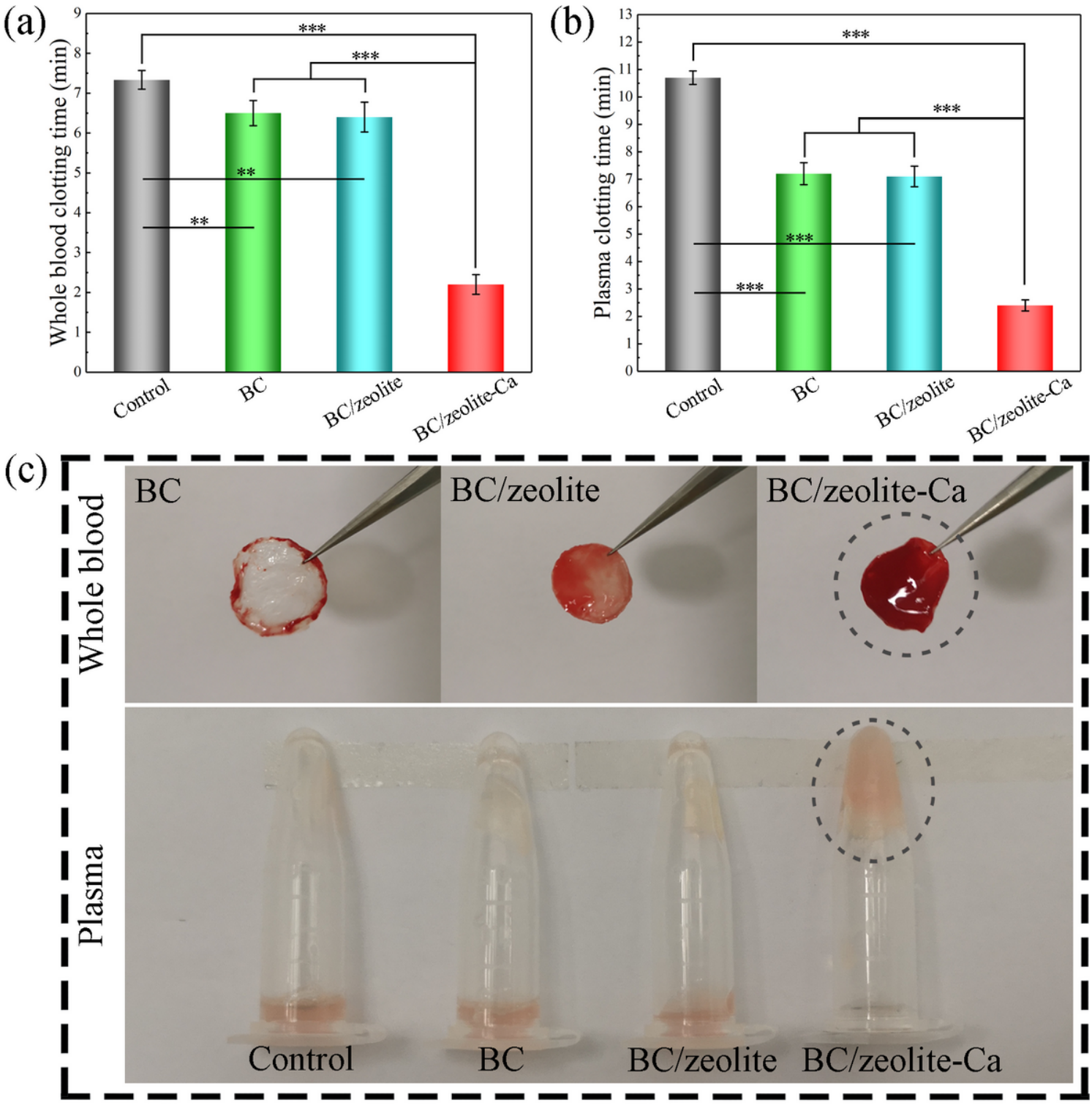

Figure 7

(a) Whole blood clotting time of BC, BC/zeolite, and BC/zeolite-Ca NFAs. (b) Plasma clotting time of BC, BC/zeolite, and BC/zeolite-Ca NFAs. (c) Optical images of whole blood clots and plasma clots forming at the test time of 2.5 min. (** and *** represent $P < 0.01$ and $P < 0.001$, respectively).

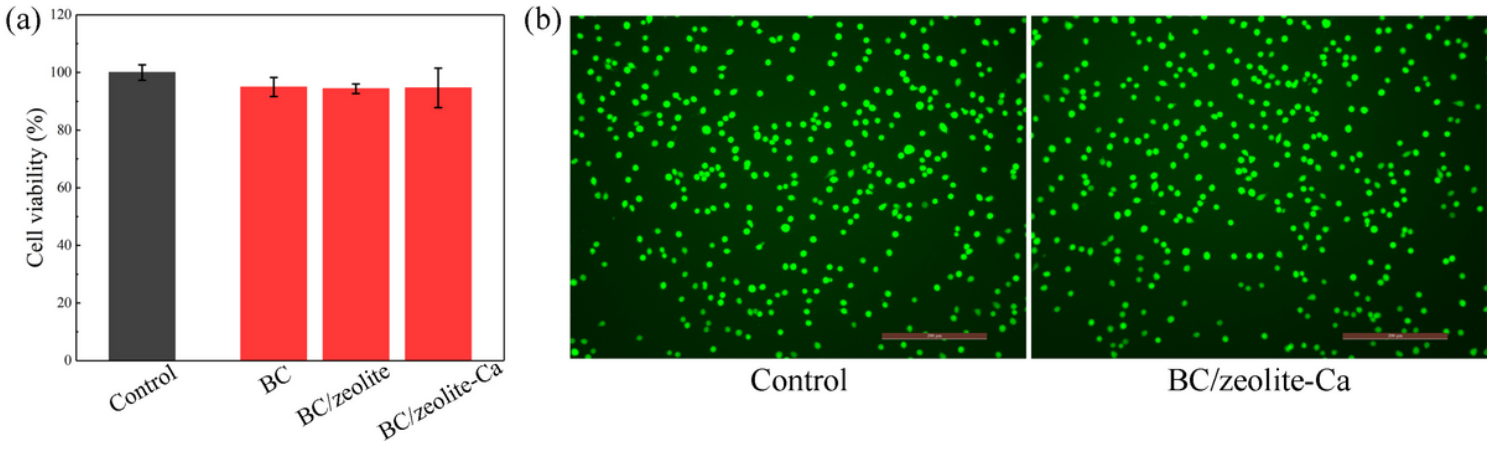

Figure 8

(a) Cell viability of BC, BC/zeolite, and BC/zeolite-Ca NFAs. (b) Fluorescence staining images of control and BC/zeolite-Ca groups.

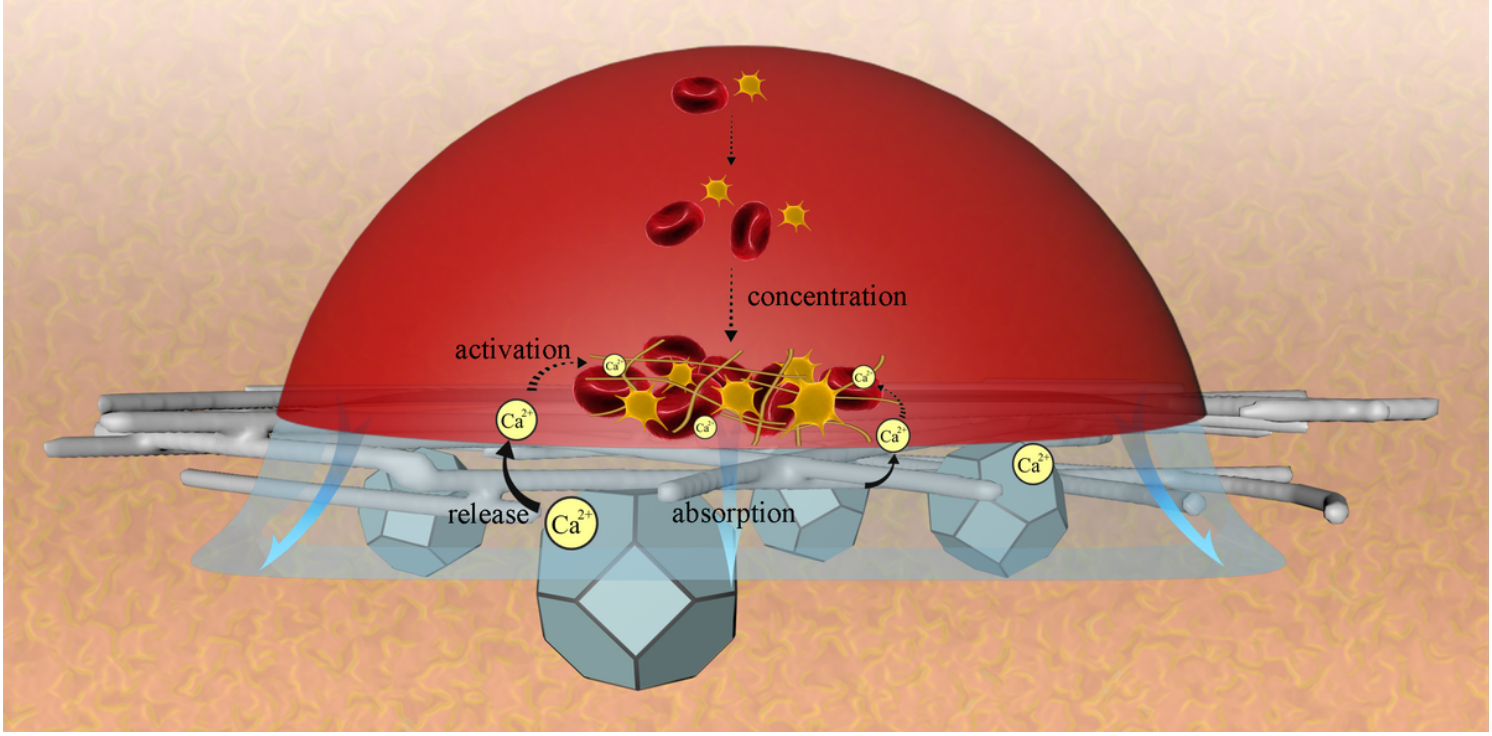

Figure 9

Schematic of the hemostatic mechanisms of BC/zeolite-Ca.